JACS
JOURNAL OF THE AMERICAN CHEMICAL SOCIETY
pubs.acs.org/JACS
Article

Crystallizing Atomic Xenon in a Flexible MOF to Probe and Understand Its Temperature-Dependent Breathing Behavior and Unusual Gas Adsorption Phenomenon

Hao Wang, Mark Warren, Jacek Jagiello, Stephanie Jensen, Sanjit K. Ghose, Kui Tan, Liang Yu, Thomas J. Emge, Timo Thonhauser, and Jing Li*

Cite This: J. Am. Chem. Soc. 2020, 142, 20088−20097

ABSTRACT: Flexible metal−organic frameworks (MOFs) hold great promise as smart materials for specific applications such as gas separation. These materials undergo interesting structural changes in response to guest molecules, which is often associated with unique adsorption behavior not possible for rigid MOFs. Understanding the dynamic behavior of flexible MOFs is crucial yet challenging as it involves weak host−guest interactions and subtle structural transformation not only at the atomic/molecular level but also in a nonsteady state. We report here an in-depth study on the adsorbate- and temperature-dependent adsorption in a flexible MOF by crystallizing atomic gases into its pores. $Mn(ina)_2$ shows an interesting temperature-dependent response toward noble gases. Its non-monotonic, temperature-dependent adsorption profile results in an uptake maximum at a temperature threshold, a phenomenon that is unusual. Full characterization of Xe-loaded MOF structures is performed by *in situ* single-crystal and synchrotron X-ray diffraction, IR spectroscopy, and molecular modeling. The X-ray diffraction analysis offers a detailed explanation into the dynamic structural transformation and provides a convincing rationalization of the unique adsorption behavior at the molecular scale. The guest and temperature dependence of the structural breathing gives rise to an intriguing reverse of Xe/Kr adsorption selectivity as a function of temperature. The presented work may provide further understanding of the adsorption behavior of noble gases in flexible MOF structures.

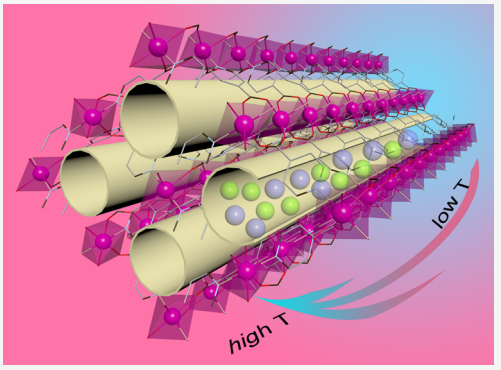

INTRODUCTION

Metal−organic frameworks (MOFs) represent a fascinating class of porous materials featuring rich structural chemistry and systematically tunable properties and functionality. Extensive investigations have been conducted on MOFs for various applications including gas separation,[1−5] molecular sensing,[6,7] catalysis,[8,9] and lighting.[10,11] Many MOFs possess rigid networks and undergo fully reversible guest adsorption−desorption processes. A small group of these materials, however, feature flexible structures and go through structural transformation under external stimuli, commonly via guest inclusion and removal. Such a transformation has rarely been observed in conventional crystalline solids such as zeolites.[12−15] Despite the fact that only 1 out of 200 reported MOFs shows markedly structural flexibility, they represent a unique type of materials possessing unexpected yet often desirable properties for specific applications.[16−18] For example, reversible structural transition of a MOF between "collapsed" and "expanded" phases toward gas adsorption and desorption can maximize its deliverable capacity or selectivity for gas storage and separation.[3,19]

The dynamic structural behavior of flexible MOFs can occur through linker rotation, swelling, and subnetwork displacement, to name a few.[16] Such structural transformations are usually accompanied by significant changes in crystal lattice parameters and pore structures, which are reflected by a peak shift in powder X-ray diffraction patterns or stepped gas adsorption isotherms. Nevertheless, in-depth characterization of these structural changes has been challenging and remains underexplored. Studies on the dynamic behavior of flexible MOF structures have largely relied on gas adsorption,[20−25] powder X-ray diffraction,[26,27] and IR/Raman spectroscopy.[28] Single-crystal X-ray diffraction (SCXRD) represents a more straightforward and powerful technique for the characterization of host−guest interactions and any associated crystallographic phase transitions. For example, it offers direct visualization of guest adsorption sites in MOFs, which is critical to the design of new, better performing materials for targeted applica-

Received: September 8, 2020
Published: November 11, 2020

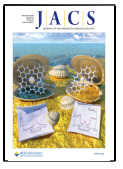

https://dx.doi.org/10.1021/jacs.0c09475
J. Am. Chem. Soc. 2020, 142, 20088−20097

tions.[29,30] However, SCXRD analysis of guest-included MOF structures is demanding. It requires the guest molecules to be strongly adsorbed (trapped) and periodically arranged so that they can be crystallographically identified. In addition, it is critical that the host structure retains single crystallinity upon activation, guest loading, and removal. This is particularly challenging for flexible MOFs since the microscopic changes in the crystal lattice accompanied by structural transformation upon guest removal and uptake often lead to macroscopic damage of single crystals. As a result, SCXRD analysis of guest−framework interactions in flexible MOFs is very limited, and their underlying dynamic structural behaviors are not well understood.[12,18,31]

The reversible phase transition of flexible MOFs in response to guest adsorption and desorption, referred to as breathing or gate opening, depends largely on the guest species and its pressure.[16] In this study, we demonstrate that temperature can also play a critical role in the structural breathing of a flexible MOF and thereby control its gas adsorption behavior. We use atomic xenon as a probe to explore and understand the dynamic phase transition of a flexible MOF structure, $Mn(ina)_2$ (ina^- = isonicotinate).[29] Xe is selected as the guest molecule since its adsorption mechanism in MOFs is underinvestigated,[32−36] and more importantly, it has been identified as a suitable probe to study the structural dynamics of the title compound through a prescreening test. The flexibility of MOF structures can bring additional benefits to gas separation, and understanding the gas adsorption behavior in flexible MOFs may help to design structures with better performance.[37−39] The temperature-dependent crystallographic phase transition of $Mn(ina)_2$ upon Xe adsorption has been examined by *in situ* single-crystal X-ray diffraction and *in situ* synchrotron powder X-ray diffraction at different temperatures. The temperature-dependent structural breathing of $Mn(ina)_2$ leads to an unusual adsorption behavior where gas uptake goes through a maximum at a temperature threshold, resulting in an intriguing reversed Xe/Kr selectivity.

EXPERIMENTAL SECTION

Synthesis of $Mn(ina)_2$. $[Mn(ina)_2](EtOH)_{0.5}$ was prepared via solvothermal synthesis using Teflon-lined 23 mL stainless steel autoclaves. A mixture of $Mn(NO_3)_2{\cdot}4H_2O$ (142 mg, 0.57 mmol) and isonicotinic acid (140 mg, 1.14 mmol) was dispersed in 18 mL of 95% ethanol. The mixture was stirred at room temperature with a stirring speed of 300 r/min for 2 h and then heated at 100 °C for 1 day. After cooling down naturally to room temperature, block shaped crystals were harvested through vacuum filtration and washed with ethanol and dried in air (60% yield based on Mn metal).

General Characterizations. Powder X-ray diffraction (PXRD) analysis was performed with a Rigaku Ultima-IV automated diffraction system using Cu Kα radiation (λ = 1.5406 Å) as the light source. The data were collected at room temperature in a 2θ range of 3−40° with a scan speed of 2°/min. The operating power was 40 kV/40 mA. Thermogravimetric analysis (TGA) was carried out on a Q5000 (TA Instruments) thermal gravimetric analyzer. For a typical measurement, ∼3 mg of sample was loaded onto a platinum pan and heated from room temperature to 600 °C with a ramp rate of 10 °C/min under nitrogen flow.

Adsorption Simulation. Adsorption simulation for Xe is performed with Materials Studio 5.0 (Accelrys) with the guest-removed crystal structure of Xe-loaded $Mn(ina)_2$. The GCMC method and Burchard Universal Force Field are employed in the modeling system. A supercell built on 4 × 4 × 4 unit cells has been created for the simulation. The simulation has been done at 298 K and 1 bar, with 10^7 calculation steps.

Adsorption Isotherms Measurements. Adsorption isotherms of various small gases at subatmospheric pressures and subambient temperatures were collected with a Micromeritics 3Flex volumetric adsorption analyzer equipped with a cryostat (Cold Edge Technologies). Isotherms at above ambient temperatures and elevated pressures up to 10 bar were measured using a Micromeritics ASAP 2050 instrument. The temperature was controlled using an Isocontroller (Micromeritics). Around 150 mg of as-synthesized $Mn(ina)_2$ sample was activated at 150 °C under dynamic vacuum overnight prior to data collection. The sample was reactivated for 2 h between each isotherm measurement.

***In Situ* Single-Crystal X-ray Diffraction Analysis.** Single-crystal X-ray diffraction experiments under Xe atmosphere were carried out at beamlines I19 at Diamond Light Source. Crystals were selected without the use of a manipulation oil as this can affect the gas uptake. A crystal was mounted on the end of a mitogen loop using a minimal amount of super glue. The mount is then inserted into the I19 beamline gas cell which consists of a 1 mm quartz capillary, Swagelok connections, and miniature quick connect. The cell is then mounted on the diffractometer and connected (via the swagelok quick connect) to the I19 gas rig with stainless steel capillary tubing. The experiments described in this article were performed without removing the cell from the diffractometer. Upon mounting, the cell and sample were flash cooled to 200 K, and an ambient collection was obtained. The crystal was activated by rising the temperature to 393 K (Cryostream ramp rate of 360 K/h) and performing three vacuum/atmospheric pressure purges using N_2. The quality of the diffraction was monitored during this process to ensure crystallinity was retained. The crystal was held under vacuum (10^{-5} mbar) at 393 K for a further 2 h. The Cryostream was ramped to 200 K before an activated structure was collected for comparison purposes. At 200 K, the evacuated cell and lines were then refilled with Xe gas (CK gas products, Xenon LB-XEN-N5.0, 99.999% purity) to 2 bar pressure (1 bar gauge pressure) using a I19 gas control rig. Data sets were then obtained at 200, 240, 275, 298, 328, and 338 K. The Cryostream was ramped at 360 K/h with a sleep period of 3 min to ensure the temperature was stable.

Data indexing and integration procedures were performed by DIALS, while data scaling and absorption correction procedures were performed by AIMLESS, all of which were implemented via Xia2. In all data sets there was the presence of a weak incommensurate reflection which could be processed using a superlattice. In this instance the resulting structure from the superlattice did not provide any additional information, and therefore a unit cell xXia2 input was used to ensure indexing from the main reflections. Single-crystal structures were solved and refined against F^2 values and by Rietveld refinement as needed. Full crystal data are provided in the Supporting Information. X-ray diffraction data were collected in the Experiments Hutch 2 (EH2) of Beamline I19, at the Diamond Light Source, using the Newport kappa-geometry four-circle diffractometer fitted with a Dectris Pilatus 300 K pixel-array photon-counting detector. Data sets consisted of six φ and Ω sweeps with step size and exposure time of 0.2° and 0.2 s, respectively.

***In situ* Synchrotron Powder X-ray Diffraction Measurements.** Freshly desolvated activated $Mn(ina)_2$ was loaded into a Kapton capillary of 1 mm diameter that was held in place at both ends with quartz wool to allow the flow of gases through. The capillary was attached to the flow cell with swagelock fittings and Teflon ferrules. Stainless steel leak-tight gas lines were attached to both sides of the flow cell. Gases (He, Xe) were passed through separate flow meters (Brooks Instruments, Hatfield, PA) with dual step pressure and volume controls and fed to a six-channel automated/programmable switching valve (VICI, Houston, TX). The outlet of the gas was fitted with another flow meter to monitor the outlet gas flow rate to the RGA. At the start of the experiment, the specimen was activated at 423 K under flowing He for more than 6 h. *In situ* XRD measurements were carried out during gas flow to monitor the dehydration process. Subsequently, Xe gas was loaded into the activated MOF at room temperature as per the experimental requirements for the gas flow rate (mostly 10 cc/min). This cycle either ended or started with a quick follow-up activation process of

https://dx.doi.org/10.1021/jacs.0c09475
J. Am. Chem. Soc. 2020, 142, 20088−20097

heating the sample at 423 K under flowing He for about an hour to purge the MOF and flow cell gas lines. In situ XRD data were collected every 10 min during each cycle. Gas-loading adsorption and desorption measurements were carried out at temperatures between 200 and 350 K for a 10 min cycle of Xe loading followed by an activation process for 30 min before each gas loading. The *in situ* powder XRD measurements were performed with synchrotron X-rays at Beamline 28-ID-2 of NSLS-II (52.38 keV, λ = 0.2362 Å). During all the experimental processes, *in situ* XRD patterns were obtained using a large 2D area detector.

Computational Details. DFT calculations were performed in Quantum ESPRESSO using the vdW-DF exchange-correlation functional in order to capture the long-range interactions imperative for guest molecule adsorption in MOFs. The Hubbard *U* correction (value of 0.24 Ry) was implemented on the Mn metal atoms to account for the on-site coulomb interactions of the d-electrons. The unit cell consisted of 108 atoms, and thus only the Γ-point was considered. We used Vanderbilt ultrasoft pseudopotentials with a wave function cutoff of 40 Ry and a density cutoff of 400 Ry. Structural relaxations were performed until the forces on the atoms were less than 1×10^{-5} Ry/bohr. Electronic relaxations were performed until SCF loops reached a convergence of 1×10^{-5} Ry. Binding energies were calculated by taking the gas@MOF total energy and subtracting the energy of relevant fragments. Energy barriers for rotating the pyridine rings were calculated using a transition-state search algorithm, i.e., the climbing-image nudged-elastic-band (NEB).

Additional information on material synthesis, characterization, adsorption data collection, and calculations can be found in the Supporting Information.

RESULTS AND DISCUSSION

Screening Study of Mn(ina)$_2$ toward the Adsorption of Small Gases. Mn(ina)$_2$ is a flexible three-dimensional (3D) framework built on a primary building unit (PBU) of octahedral MnO_4N_2 with each octahedron connected to two pyridyl nitrogen and four carboxylates from six different ina$^-$ linkers. The framework possesses one-dimensional (1D) channels along the crystallographic *a* axis (Figure 1). As-

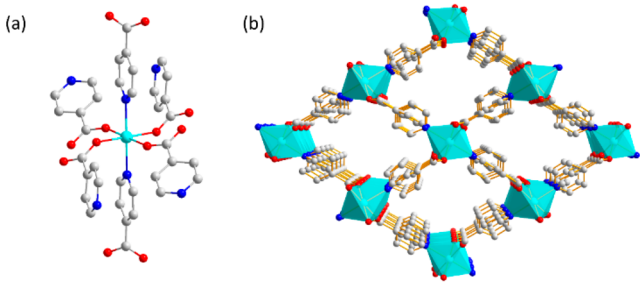

Figure 1. Crystal structure of Mn(ina)$_2$. (a) Primary building unit of Mn(ina)$_2$ showing the coordination mode of Mn cation. (b) Structure representation of Mn(ina)2 showing the 1D channel. Color scheme: Mn (cyan), O (red), N (blue), C (gray); hydrogen atoms are omitted for clarity.

synthesized Mn(ina)$_2$(EtOH)$_{0.5}$ sample was prepared according to the reported procedure with slight modifications (Figures S1 and S2). We first conducted a screening study of the adsorption of various small gases in Mn(ina)$_2$ at 298 K and up to 1 bar, including CO_2, CH_4, C_3H_6, C_3H_8, Xe, and Kr. Mn(ina)$_2$ exhibits structural breathing upon loading and unloading of certain gases, as suggested by the characteristic profiles of selected gas adsorption isotherms (Figure S3). The adsorption profiles are highly dependent on the type of adsorbates and may be classified into three categories. CH_4 and Kr represent the first category where the adsorption isotherms are almost linear and the adsorbed amounts are negligible (Figure S3b/f). This is due to their small molecular/atomic size and/or nonpolar nature, which lead to relatively weak adsorbent−adsorbate interaction that is not sufficient to induce the structural transformation up to 1 bar at the given temperature. The adsorption of CO_2, which falls into the second category, displays a stepwise profile which is commonly observed for flexible MOFs:[27] a linear increase up to ∼0.8 bar and a steep rise at 0.8−0.9 bar followed by a plateau up to 1 bar, indicating that Mn(ina)$_2$ undergoes a structural change at ∼0.8 bar of CO_2 (Figure S3a). The notable adsorption of CO_2 at pressure before 0.8 bar suggests that the gas can diffuse into the channel of the MOF even before the gate opens. The third category, including C_3H_6, C_3H_8, and Xe, exhibits stepped adsorption isotherms as well but with lower gate-opening pressure (0.25 bar for Xe, <0.01 bar for C_3H_6 and C_3H_8, Figure S3c/d/e). However, different from CO_2, these gases show essentially no adsorption before the MOF opens its gate. This indicates that the framework prior to structural change is porous toward smaller molecules such as Kr, CH_4, and CO_2 (also possibly adsorbed at the pore mouth or defect sites) but would not accommodate gases of larger size including C_3H_6, C_3H_8, and Xe. Since the gate-opening pressure of Xe falls into a more attainable pressure range for the current study, it offers an easy accessibility to experimentally investigate the adsorption behavior and structural dynamics of Mn(ina)$_2$. With Xe as an atomic probe, we have performed a comprehensive study of its adsorption over a wide range of temperature (200−350 K), its crystallization in the MOF channels, and the underlying structural transformation of the MOF as a result of Xe loading and the change of temperature.

Crystallization of Xe in Mn(ina)$_2$. Combined techniques including molecular modeling, IR/Raman spectroscopy, neutron scattering, synchrotron X-ray, and neutron diffraction are commonly applied to understand adsorbate−adsorbent interaction.[16] Compared to these indirect techniques, single-crystal X-ray diffraction is capable of providing the most straightforward and direct information on adsorbed molecules and induced structural changes for flexible MOFs. However, as pointed out earlier, the determination of crystal structures of adsorbate-included MOFs is very difficult. It can be even more challenging for flexible MOFs as the structural changes upon guest uptake and removal are not only dynamic but also can easily lead to the fragmentation of single crystals.[12,18] Fortunately, Mn(ina)$_2$ represents a very robust flexible MOF that retains its single crystallinity under repeated guest loading and removal, allowing a direct visualization of its structural transformation by single-crystal X-ray diffraction analysis.

In the pristine structure of Mn(ina)$_2$(EtOH)$_{0.5}$, the open channels are not cylindrical but segmented, comprised of repeating chambers and necks (Figure 2a). They are decorated by pyridine rings, and clearly the orientation of these aromatic rings influences the pore geometry. The chambers, where the initial solvent molecules (ethanol) reside, are surrounded by four pyridine rings that are roughly parallel to the channel direction, whereas the necks are the regions composed of four pyridine rings that are approximately perpendicular to the channel. The necks have the smallest pore width of 2.0 Å, which is too narrow for ethanol molecules to fit in, and thus they only stay in the chambers. Removal of the ethanol molecules by activating the as-synthesized crystals at 120 °C under vacuum yields the activated phase, Mn(ina)$_2$. The activated compound crystallizes in space group $P2_1/c$, the same

https://dx.doi.org/10.1021/jacs.0c09475
J. Am. Chem. Soc. 2020, 142, 20088−20097

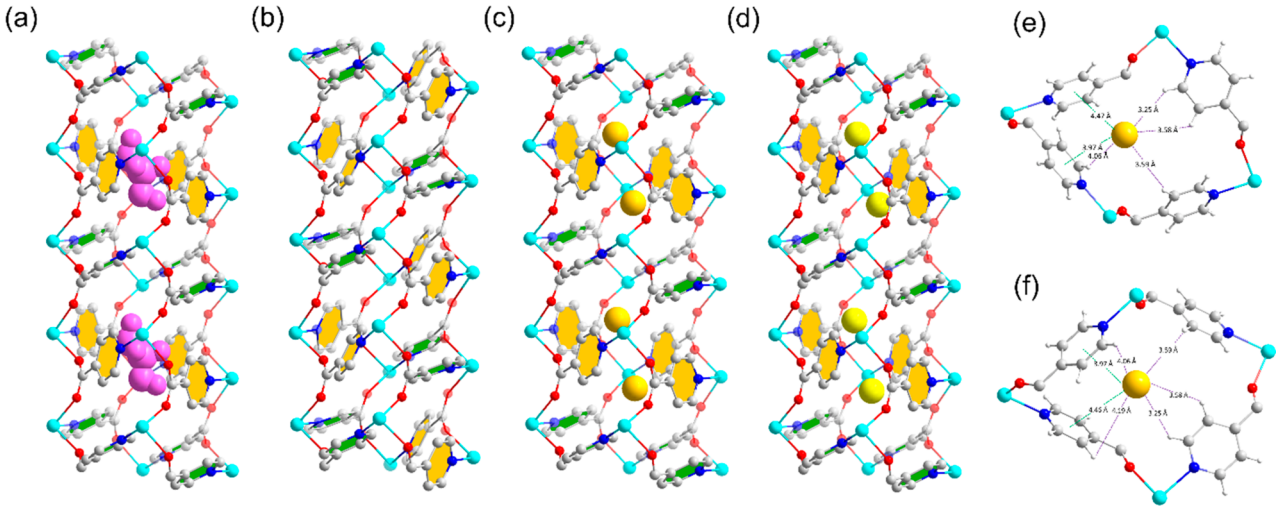

Figure 2. Cystallization of Xe in $Mn(ina)_2$. Crystal structures of (a) as-synthesized Mn(ina)2·0.5EtOH, (b) activated Mn(ina)2, (c) simulated Xe-loaded $Mn(ina)_2$, and (d) experimental Xe-loaded Mn(ina)2. (e) and (f) Xe adsorption sites in $Mn(ina)_2$. Color scheme: Mn (cyan), O (red), N (blue), C (gray), H (white). Purple spacefill models represent ethanol, and yellow/gold spheres represent Xe atoms. Green- and orange-colored hexagons represent pyridine rings that are roughly perpendicular and parallel to the channel, respectively.

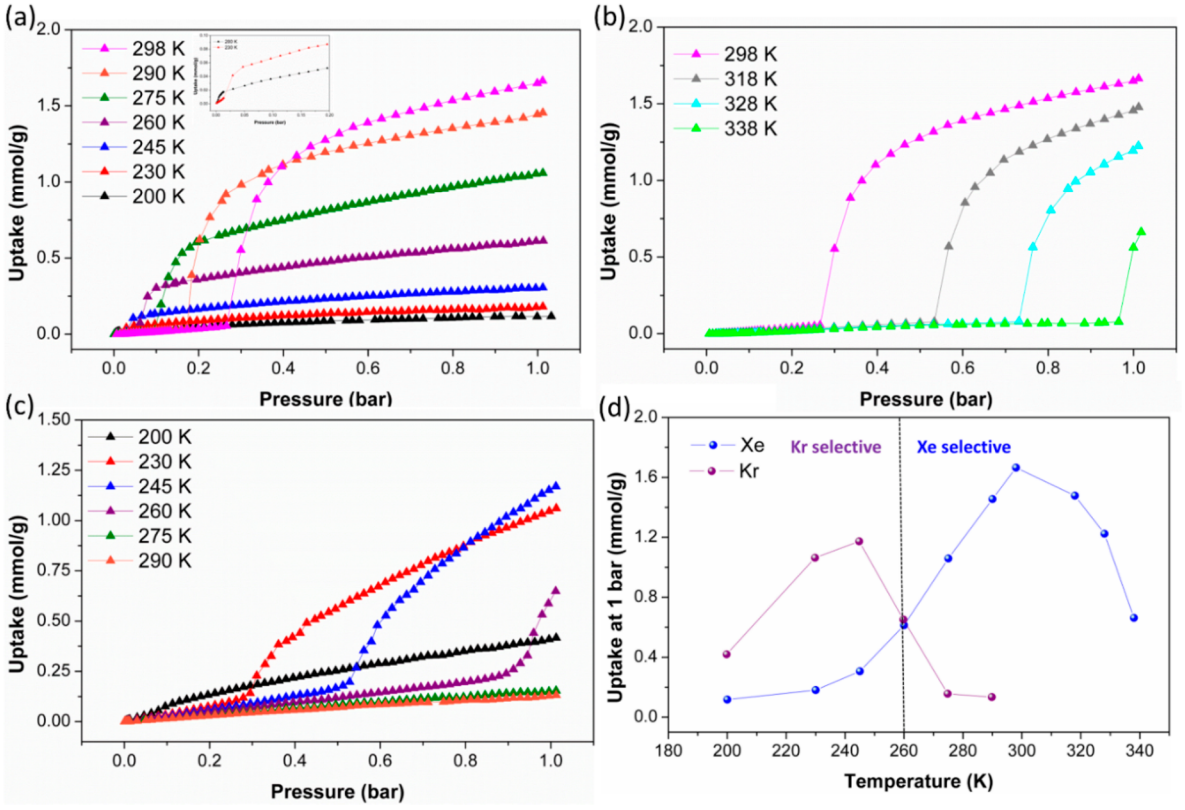

Figure 3. Adsorption of Xe and Kr in $Mn(ina)_2$. (a) Xe adsorption isotherms at 200−298 K. Insert: isotherms at 200 K (black) and 230 K (red) at low pressure showing gate opening. (b) Xe adsorption isotherms at 298−338 K. (c) Kr adsorption isotherm at 200−290 K. (d) Uptake amounts of Xe (blue) and Kr (purple) as a function of temperature at a fixed pressure (1 bar). For Xe and Kr sorption isotherms, desorption branches are omitted for clarity. See the Supporting Information for details.

as the as-synthesized material, and its overall connectivity is the same as that of the original structure. However, a structural transformation occurs upon guest removal involving rotation and rearrangement of pyridine rings (Figure 2b and Figure S4), which leads to a striking change in the pore geometry. In the activated structure, the original neck-chamber connections disappear whereas each channel segment is surrounded by two pyridine rings perpendicular to the channels and the other two parallel to the channels. This closes up the chambers and results in shrinkage in pore size. The contracted channel is too small to accommodate large molecules such as propane, propylene, or Xe but can adsorb a moderate amount of smaller guests such as CO_2, as indicated by their adsorption isotherms (Figure S3).

https://dx.doi.org/10.1021/jacs.0c09475
J. Am. Chem. Soc. 2020, 142, 20088−20097

By looking into the structure features of the as-synthesized and activated compounds including their neck and chamber sizes, we speculated that the guest-free structure $Mn(ina)_2$ must transform back to the original form in order to accommodate larger guests such as Xe atoms, which would likely reside at the chamber sites. To experimentally confirm our hypothesis, we attempted to structurally characterize Xe-loaded compound via single-crystal X-ray diffraction analysis. After the as-synthesized crystals were activated at 120 °C under vacuum, the sample cell was filled by pure Xe gas to 1 bar, and the crystals were kept under Xe atmosphere at 298 K for a sufficiently long time to ensure adsorption equilibrium was reached. The crystals were subsequently subject to X-ray diffraction analysis. The results reveal that the crystal structure of the Xe-loaded sample $Mn(ina)_2Xe_{0.82}$ adopts the same space group and connectivity as the as-synthesized form with similar segmented channels and alternating chambers and necks, confirming that the activated structure undergoes a transformation back to the original as-synthesized structure in order to accommodate Xe atoms into its pore space. Apparently, the structural transformation involves the rotation and rearrangement of the pyridine rings as a result of the gas−framework interaction. Interestingly, the structure of $Mn(ina)_2Xe_{0.82}$ appears to be more porous than that of the as-synthesized $Mn(ina)_2(EtOH)_{0.5}$, as its calculated surface area (249 m^2/g) is larger than that of the latter (158 m^2/g). $Mn(ina)_2Xe_{0.82}$ also possesses a larger unit cell (unit cell volume 1378 vs 1346 $Å^3$). This indicates that the structural transformation is guest-dependent. As expected, Xe atoms reside at the chamber sites, leaving the necks unoccupied (Figure 2c). Each chamber is able to accommodate two Xe atoms with a Xe−Xe distance of 4.08 Å. The simulated Xe-adsorbed structure by molecular modeling agrees well with that determined by SCXRD (Figure 2d), in terms of both uptake amount and adsorption sites of Xe. Physically adsorbed Xe atoms interact with the channel wall (hydrogen atoms and pyridine rings) through van der Waals interactions. This represents a rare example of the study of temperature-dependent structure dynamics using atomic gas as a probe.[33,36]

Unusual Temperature-Dependent Adsorption of Xe and Kr. Xe adsorption isotherms collected at various temperatures exhibit an abnormal yet very interesting phenomenon: The adsorption capacity of Xe goes through a maximum as a function of temperature from 200 to 338 K (Figure 3, Figures S5−S7). For a given temperature, there is essentially no Xe adsorption at low pressure (before structural transformation), indicating that the pore size of the activated structure is too small for Xe atoms to fit in, as discussed earlier. When the applied pressure reaches a threshold, the gate begins to open, where the adsorption isotherm shows a steep increase and then slowly levels out to a plateau up to 1 bar. The equilibrium uptake amount at 1 bar, however, follows a reversed order with respect to the normal behavior of gas adsorption for all isotherms collected at and below 298 K. Above 298 K, the normal adsorption behavior is observed. Therefore, Xe uptake reaches a maximum at 298 K as the temperature increases from 200 to 338 K. Also noted is the increase of the gate-opening pressure as a function of increasing temperature, which is observed over the entire temperature range studied (200−338 K). This observation is not unusual and is a common phenomenon for flexible MOFs. As generally recognized, gate opening is a result of gas−framework interaction, and at lower temperature Xe atoms interact more strongly with the framework so that a lower pressure is needed to induce the gate opening.

As for the adsorption of Kr in $Mn(ina)_2$, we speculated that gate opening will eventually occur if the pressure continues to increase or the temperature continues to decreases. High-pressure adsorption measurements at ambient temperature indeed confirm our hypothesis, and gate opening for Kr takes place at ∼1, 3, and 6 bar and at 275, 293, and 338 K, respectively (Figure S8). Kr adsorption isotherms at low temperatures also reveal a temperature-dependent adsorption where the adsorbed amount goes through a maximum at 245 K, in a similar fashion to that of Xe (Figure S9). Temperature-dependent adsorption of Xe and Kr in $Mn(ina)_2$ leads to intriguing temperature-dependent Xe/Kr adsorption selectivity, as shown in Figure 3d. The compound is Xe selective at high temperatures (T > 260 K) whereas it preferentially adsorbs Kr at lower temperatures (T < 260 K). At T > 260 K, Kr is not able to induce gate opening at a pressure up to 1 bar, and thus the adsorbed amount is negligible. In contrast, due to the stronger interaction of Xe with the framework, it triggers gate opening at a relatively low pressure, and thus a large amount of Xe is adsorbed at 1 bar. Therefore, in this temperature range, the material shows a high Xe/Kr selectivity. This is expected considering the differences in the atomic size (kinetic diameter: 4.05 vs 3.65 Å) and polarizability (40.4 vs 24.8 × $10^{25}/cm^3$) of Xe and Kr. Gate opening is a response of the MOF framework to its interaction with guest molecules. The higher the interaction energy, the lower the force of a gas molecule that will be required to trigger the gate opening. Such phenomenon has been commonly observed in the adsorption of many other gases on flexible MOFs. The higher adsorption affinity of Xe to the framework makes it easier to induce the gate opening, resulting in a lower gate-opening pressure.[40,41] To estimate the separation performance of $Mn(ina)_2$ on binary mixtures of Xe and Kr, we obtained IAST Xe/Kr selectivities for several compositions at room temperature. As shown in Figure S19, in all cases, the values are higher than 100 over the entire pressure range.

To confirm this hypothesis, we calculated the adsorption enthalpies of Xe and Kr at the gate-opening inflection point (Figure S10). The results indicate that the guest-induced structural transformation of $Mn(ina)_2$ follows a simple thermodynamic relationship between the temperature and pressure of gate opening, and the adsorption enthalpies for Xe and Kr are 26.5 and 17.9 kJ/mol, respectively, consistent with the aforementioned observations. The strong interaction between Xe atoms and the channel can be attributed to the tailored pore shape and size that fit favorably for Xe atoms. At the low-temperature region (T < 260 K), in contrast, gate opening occurs at relatively low pressure for both Xe and Kr. However, as the gate is only partially open, Kr is preferably adsorbed due to its smaller atomic size and less diffusion restrictions. This is an interesting case since porous materials that are Kr-selective have rarely been reported.[42] Yet the phenomenon itself is not unexpected considering the fact that Xe is more polarizable; thus, it usually exhibits a stronger interaction with the pore surface of materials that can adsorb both Xe and Kr.

Temperature-Dependent Structural Breathing. Based on the aforementioned observations, we thus propose a temperature-dependent breathing mechanism upon Xe adsorption (Figure 4). At lower temperatures (T < 298 K), Xe−framework interactions are sufficiently high to push the gate

https://dx.doi.org/10.1021/jacs.0c09475
J. Am. Chem. Soc. 2020, 142, 20088−20097

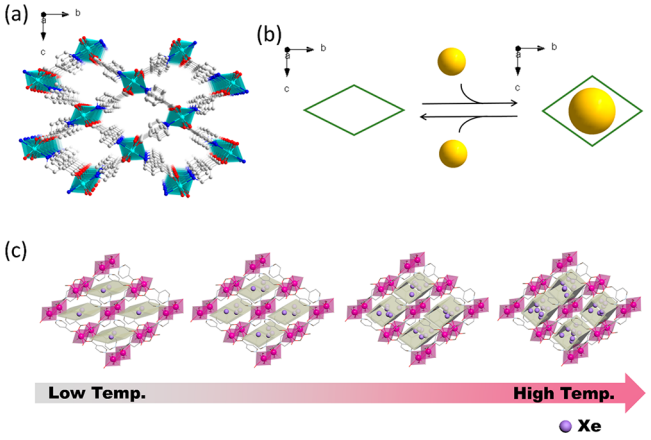

Figure 4. Proposed mechanism for the structural change of $Mn(ina)_2$. (a) Perspective view of the 1D channel along the *a* axis. (b) Schematic demonstration of the change of the channel geometry upon adsorption of guest molecules. Green rhombus outlines the channel in $Mn(ina)_2$. (c) Schematic presentation of the proposed temperature-dependent gate-opening process. The channels are shaded in gray.

partially open to accommodate some gases into the pore. The extent of the gate opening is temperature dependent under Xe atmosphere, and as temperature increases, the gate is opened further so that more gases are adsorbed. The gate is fully opened when the temperature reaches 298 K, giving rise to a maximum uptake at this temperature. As the temperature continues to increase (T > 298 K), the adsorption behavior reverses back to normal (namely uptake amount decreases as temperature increases) since the pore space remains constant.

To experimentally evaluate the structure changes of $Mn(ina)_2$ upon Xe/Kr adsorption, *in situ* synchrotron X-ray diffraction studies have been performed. Data were collected with high-energy beam (52 keV, λ = 0.2362 Å). We first evaluated possible structural variation caused by Kr adsorption, and the results are shown in Figure S11. No notable structural change was observed under Kr atmosphere, and the patterns are almost identical to that of the activated compound except for a few tiny mismatches at higher angles probably due to the inclusion of a small amount of Kr gas (without inducing gate opening). This is consistent with the adsorption results that Kr would not induce the gate opening of $Mn(ina)_2$ at ambient temperature and pressure. The scenario is different for Xe (Figure S12). When an activated sample of $Mn(ina)_2$ is placed under Xe atmosphere, the structure quickly transforms to a completely different one and keeps unchanged as time goes on. This indicates that at room temperature 1 atm of Xe would rapidly induce the gate opening of $Mn(ina)_2$ and therefore cause its structural change. The 30 consecutive patterns (with a time interval of 10 min) are essentially the same, suggesting the adsorption kinetics would not give rise to additional structural change of $Mn(ina)_2$.

To confirm our proposed temperature-dependent breathing mechanism, we carried out temperature variable *in situ* synchrotron X-ray diffraction studies on $Mn(ina)_2$ under 1 bar Xe atmosphere. The measurements were done under Xe atmosphere from 200 to 350 K (Figure 5). It is clear that the structure transforms from narrow-pore structure (activated $Mn(ina)_2$) to wide-pore structure even at temperature as low as 200 K (Figure S13). This agrees with the Xe adsorption isotherm at 200 K where the adsorbed amount is low but stepped adsorption behavior is clearly observed, indicating the occurrence of structural transformation (Figure S6). This finding suggests that the compound adopts its wide-pore structure when exposed to Xe atmosphere at all temperatures studied (200–350 K). However, the structure transformation is not complete at low temperatures as the pore is not fully open. The process would continue as a function of increasing temperature until the gate is fully open. This is verified by comparing the *in situ* PXRD patterns at different temperatures (Figure 5). Notable peak shifts have been observed as the temperature increases from 200 to 350 K. The (100) peak does not display much change, indicating that the length of the

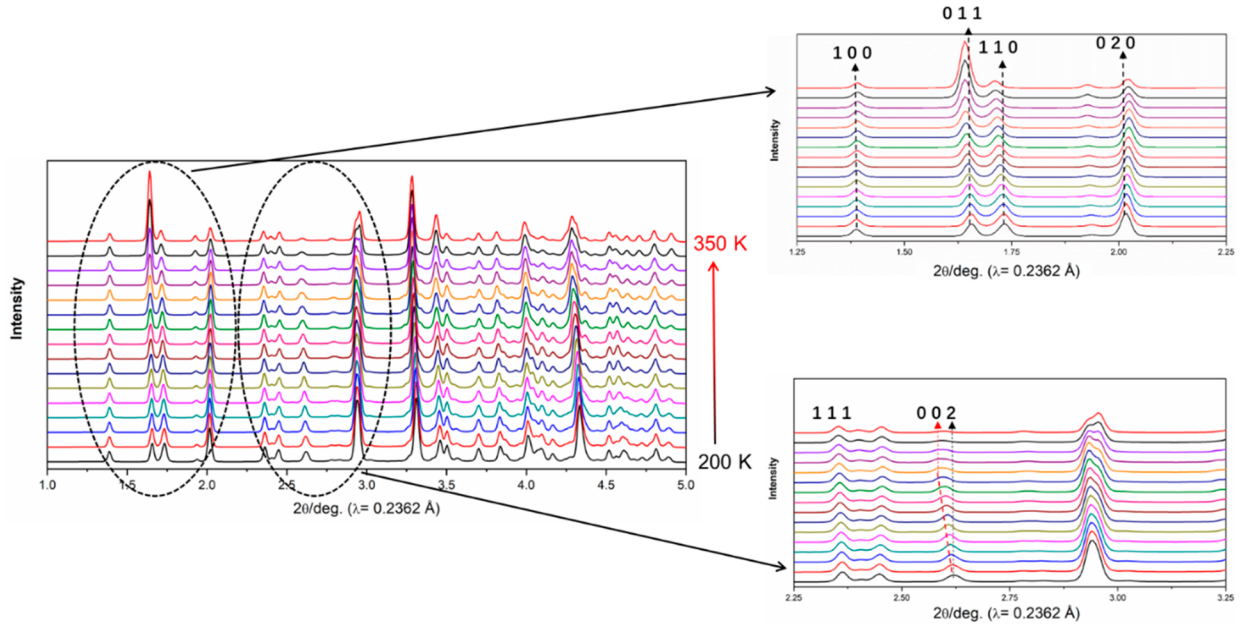

Figure 5. *In situ* PXRD analysis of $Mn(ina)_2$ under Xe atmosphere. From bottom to top, patterns collected under Xe atmosphere from 200 to 350 K with a temperature interval of 10 K. Beam energy 52.38 keV, λ = 0.2362 Å.

https://dx.doi.org/10.1021/jacs.0c09475
J. Am. Chem. Soc. 2020, 142, 20088–20097

a axis remains almost unaltered as temperature increases. This is not unexpected considering the fact that the channel is along the *a* axis. Further, the structural change is associated with the rotation of the pyridine rings which mainly relates to the *bc* plane while the *a* axis (related to the channel length) is less influenced. This is confirmed by the notable peak shifts of (020) and (002). It is noteworthy that the peak associated with the (020) crystal plane is moving toward a higher angle as temperature increases while the peak associated with the (002) plane is shifting toward a lower angle, suggesting the decrease of the *b* axis length and increase of the *c* axis length. The peak shifts, or essentially the changes in the lengths of the *b* and *c* axis, are clearly related to the change of pore geometry and result in the transformation of the channel cross section from a rhombus to a square (Figure 4). This would enlarge the effective channel diameter and further open the pore. The enlargement of the *c* axis length correlates closely to the Xe adsorption results. The structural change takes place mainly from 210 to 300 K, well consistent with our proposed temperature-dependent gate-opening mechanism derived from the adsorption behavior: As the structural transformation is occurring from 210 to 300 K, the pore in the MOF structure continues to open to adsorb more Xe gas at relatively high temperature. At temperatures above 300 K, structural transformation is complete, and the pore size stays constant so that the adsorption behavior follows a typical thermodynamic process. It is worthwhile to note that temperature variable XRD measurements on an activated $Mn(ina)_2$ sample indicate that the crystal structure remained unchanged as temperature increased from 200 to 393 K (Figure S14). This suggests that temperature change alone would not induce the structural transformation, which confirms that the dynamic structural breathing is a result of the synergetic effect of gas adsorption and temperature.

To confirm the results from temperature-dependent adsorption studies and to obtain more direct information about the temperature-dependent structural change upon Xe adsorption, we collected single-crystal data of Xe loaded $Mn(ina)_2$ at different temperatures (200, 240, 275, and 298 K) through temperature variable *in situ* single-crystal X-ray diffraction. While the space group of the structure remains the same as $P2_1/c$ at all temperatures, the unit cell volume increases from 1287.79 Å^3 at 200 K, to 1335.44 Å^3 at 275 K, and finally to 1378.49 Å^3 at 298 K, indicating a gradual swelling of the unit cell up to 7% as a result of the increase of temperature and uptake amount of Xe gases. Consistent with the *in situ* synchrotron PXRD results, a notable increase in the *c* axis (from 9.66 Å at 200 K to 10.49 Å at 298 K) and decrease in the *b* axis (13.79 Å at 200 K to 13.47 Å at 298 K) is observed (Table 1). The evolution of the *c* axis length is in good agreement with gas adsorption results (Figure 6) which once again confirm our proposed mechanism. More convincingly, the calculated pore volume and surface area of the Xe-loaded $Mn(ina)_2$ crystal structure display a notable monotonic increase as temperature increases (Table 1), confirming our proposed mechanism that the effective pore size of MOF structure is enlarging under Xe atmosphere as a function of the increasing temperature which leads to the unusual adsorption behavior. A close look at the crystal structures at different temperatures clearly reveals the evolution of the rotations of pyridine rings, which leads to a continuing increase of the dihedral angles between the two planes of the adjacent pyridine rings (Figures S15–S16) from 200 to 298 K.

Table 1. Crystal and Porosity Data for the Xe-Loaded $Mn(ina)_2$ Structure at 200, 240, 275, and 298 K

	Xe-loaded $Mn(ina)_2$ 200 K	Xe-loaded $Mn(ina)_2$ 240 K	$Mn(ina)_2Xe_{0.21}$ 275 K	$Mn(ina)_2Xe_{0.82}$ 298 K
a (Å)	9.88	9.88	9.77	10.07
b (Å)	13.79	13.76	13.63	13.47
c (Å)	9.66	9.74	10.26	10.49
α (deg)	90	90	90	90
β (deg)	101.65	101.92	102.42	104.35
γ (deg)	90	90	90	90
V (Å^3)	1288.10	1295.73	1335.44	1378.49
space group	$P2_1/c$	$P2_1/c$	$P2_1/c$	$P2_1/c$
V_p (Å^3)[a]	181	185	210	382
SA (m^2/g)[b]	118	120	136	249
pore size (Å)[c]	3.66	3.96	4.16	4.22

[a]V_p = Calculated pore volume per unit cell. [b]SA = calculated surface area (with a 1 Å probe atom). [c]Pore size measured from single-crystal structure.

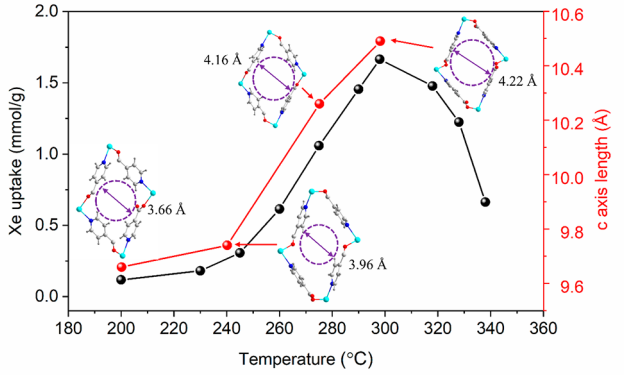

Figure 6. Changes of Xe uptake and *c* axis length as a function of temperature. Black curve (to the axis on the left) shows the Xe-adsorbed amount under 1 bar Xe gas at temperatures from 200 to 340 K. Red curve (to the axis on the right) demonstrates the change of *c* axis length under Xe atmosphere from 200 to 298 K (data derived from *in situ* single-crystal XRD results). The pore dimensions measured from the Xe-loaded single-crystal structures at different temperatures are indicated in the figure.

Accordingly, the effective pore size changes from 3.66 Å at 200 K to 4.22 Å at 298 K (Figure S17). These changes of structural parameters are in good agreement with the observed adsorption behaviors.

DFT Calculation Results. In the above sections we have demonstrated how structural deformation of $Mn(ina)_2$ takes place upon the adsorption of noble gases through single-crystal X-ray diffraction studies. We show that such structural changes involve the rotation of pyridine rings on the ina^- ligands as the gate opens and closes (Supporting Information Movie S1). To gain further understanding of the gate-opening process upon the adsorption of Xe and Kr, in particular the energy involved during the gate-opening transition,[43] we first calculated energy barriers for opening the gate with and without atomic gases. The binding energies of Xe and Kr atoms to the MOF (in its pore-open form) are −0.52 and −0.44 eV for Xe and Kr, respectively, indicating that Xe binds to $Mn(ina)_2$ more strongly than Kr. This result is consistent with the fact that Xe has a higher adsorption affinity than Kr, as obtained experimentally from their adsorption isotherms. The energy

https://dx.doi.org/10.1021/jacs.0c09475
J. Am. Chem. Soc. 2020, 142, 20088−20097

barriers to open the gate from the pore-closed form to the pore-open form were then calculated along the pathways. The results indicate that the energy barrier is the lowest when Xe atoms are uploaded to the MOF, followed by Kr, and then the activated MOF has the largest energy barrier (Figure S18). This again agrees well with the fact that the higher the adsorption energy, the lower the barrier for gate opening.

CONCLUSION

$Mn(ina)_2$ exhibits an unusual and very interesting adsorption behavior where the uptake capacity of Xe gas goes through a maximum as a function of temperature, due to its structural flexibility. A continuous structural transformation (or gate opening) is observed under Xe atmosphere as the temperature increases from 200 to 298 K, which leads to the unique yet unusual adsorption behavior: The uptake amount of Xe increases as a function of increasing temperature within a given temperature range. This phenomenon can be attributed to the synergistic effect of temperature and gas loading on a flexible MOF, for which the associated structural changes and their effect on adsorption behaviors are fully characterized by analyzing Xe-crystallized $Mn(ina)_2$ employing *in situ* single-crystal and synchrotron X-ray diffraction techniques. These studies reveal that such structural changes involve mainly the rotation and rearrangement of pyridine rings from the ina^- ligands. The temperature- and adsorbate-dependent structural transformation also leads to the temperature-dependent Xe/Kr adsorption selectivity. The MOF material is Kr selective at low temperature (T < 260 K) and becomes Xe selective at high temperature (T > 260 K), giving the highest value for Xe/Kr among all MOFs reported to this date.

While a number of flexible MOF structures have been studied and reported, very few are fully characterized by crystallographic analysis, especailly in gas-loaded forms. These materials often exhibit very interesting and unusual adsorption behavior associated with structure changes, yet the underlying mechanism of structural transformations remains largely unknown and related structure−property correlation awaits to be explored. In this work we are able to fully reveal the structural transformation mechanism of $Mn(ina)_2$ and explain its unusual adsorption phenomenon resulting from the structural flexibility by single-crystal X-ray diffraction analysis on Xe-loaded $Mn(ina)_2$ single crystals. Additionally, we have investigated the structure−property relationship in detail at the molecular level through various techniques. This study contributes to an in-depth understanding of adsorbate−adsorbent interactions and associated dynamic behavior of flexible MOFs which is important for the design of smart materials for targeted applications.

ASSOCIATED CONTENT

Supporting Information

The Supporting Information is available free of charge at https://pubs.acs.org/doi/10.1021/jacs.0c09475.

Crystallographic data, PXRD patterns, TGA data, IR spectra, and adsorption isotherms (PDF)

Rotation of pyridine rings on the ina^- ligands as the gate opens and closes (MP4)

Crystallographic data for $C_{12}H_8MnN_2O_4$, 200 K/vacuum (CIF)

Crystallographic data for $C_{12}H_8MnN_2O_4$, 200 K/1 bar Xe (CIF)

Crystallographic data for $C_{12}H_8MnN_2O_4$, 240 K/1 bar Xe (CIF)

Crystallographic data for $C_{12}H_8MnN_2O_4Xe_{0.23}$, 275 K/1 bar Xe (CIF)

Crystallographic data for $C_{12}H_8MnN_2O_4Xe_{0.82}$ (CIF)

AUTHOR INFORMATION

Corresponding Author

Jing Li − *Department of Chemistry and Chemical Biology, Rutgers University, Piscataway, New Jersey 08854, United States; Hoffmann Institute of Advanced Materials, Shenzhen Polytechnic, Shenzhen, Guangdong 518055, China;* orcid.org/0000-0001-7792-4322; Email: jingli@rutgers.edu

Authors

Hao Wang − *Hoffmann Institute of Advanced Materials, Shenzhen Polytechnic, Shenzhen, Guangdong 518055, China; Department of Chemistry and Chemical Biology, Rutgers University, Piscataway, New Jersey 08854, United States;* orcid.org/0000-0001-7732-778X

Mark Warren − *Diamond Light Source, Harwell Science and Innovation Campus, Didcot OX11 0DE, United Kingdom*

Jacek Jagiello − *Micromeritics Instrument Corporation, Norcross, Georgia 30093, United States*

Stephanie Jensen − *Department of Physics and Center for Functional Materials, Wake Forest University, Winston-Salem, North Carolina 27109, United States*

Sanjit K. Ghose − *National Synchrotron Light Source II, Brookhaven National Laboratory, Upton, New York 11973, United States*

Kui Tan − *Department of Materials Science & Engineering, University of Texas at Dallas, Richardson, Texas 75080, United States;* orcid.org/0000-0002-5167-7295

Liang Yu − *Hoffmann Institute of Advanced Materials, Shenzhen Polytechnic, Shenzhen, Guangdong 518055, China*

Thomas J. Emge − *Department of Chemistry and Chemical Biology, Rutgers University, Piscataway, New Jersey 08854, United States*

Timo Thonhauser − *Department of Physics and Center for Functional Materials, Wake Forest University, Winston-Salem, North Carolina 27109, United States;* orcid.org/0000-0003-4771-7511

Complete contact information is available at: https://pubs.acs.org/10.1021/jacs.0c09475

Author Contributions

The manuscript was written through contributions of all authors.

Notes

The authors declare no competing financial interest.

ACKNOWLEDGMENTS

H.W., J.L., S.J., K.T., and T.T. thank the U.S. Department of Energy, Office of Science, Office of Basic Energy Sciences for its generous support (it started under Award No. DE-FG02-08ER46491 and finished under Award No. DE-SC0019902). H.W. and L.Y. are also thankful for the partial financial support by the National Natural Science Foundation of China (21901166), the Guangdong Natural Science Foundation (2019A1515010692), as well as the Scientific and Technical

Innovation Council of Shenzhen (No. JCYJ20190809145615620).

REFERENCES

(1) Cui, X.; Chen, K.; Xing, H.; Yang, Q.; Krishna, R.; Bao, Z.; Wu, H.; Zhou, W.; Dong, X.; Han, Y.; Li, B.; Ren, Q.; Zaworotko, M. J.; Chen, B. Pore chemistry and size control in hybrid porous materials for acetylene capture from ethylene. *Science* **2016**, *353*, 141−144.

(2) Yang, S.; Ramirez-Cuesta, A. J.; Newby, R.; Garcia-Sakai, V.; Manuel, P.; Callear, S. K.; Campbell, S. I.; Tang, C. C.; Schröder, M. Supramolecular binding and separation of hydrocarbons within a functionalized porous metal-organic framework. *Nat. Chem.* **2015**, *7*, 121−129.

(3) Wang, H.; Dong, X.; Lin, J.; Teat, S. J.; Jensen, S.; Cure, J.; Alexandrov, E. V.; Xia, Q.; Tan, K.; Wang, Q.; Olson, D. H.; Proserpio, D. M.; Chabal, Y. J.; Thonhauser, T.; Sun, J.; Han, Y.; Li, J. Topologically guided tuning of Zr-MOF pore structures for highly selective separation of C6 alkane isomers. *Nat. Commun.* **2018**, *9*, 1745.

(4) McDonald, T. M.; Mason, J. A.; Kong, X.; Bloch, E. D.; Gygi, D.; Dani, A.; Crocellà, V.; Giordanino, F.; Odoh, S. O.; Drisdell, W. S.; Vlaisavljevich, B.; Dzubak, A. L.; Poloni, R.; Schnell, S. K.; Planas, N.; Lee, K.; Pascal, T.; Wan, L. F.; Prendergast, D.; Neaton, J. B.; Smit, B.; Kortright, J. B.; Gagliardi, L.; Bordiga, S.; Reimer, J. A.; Long, J. R. Cooperative insertion of CO2 in diamine-appended metal-organic frameworks. *Nature* **2015**, *519*, 303−308.

(5) Nugent, P.; Belmabkhout, Y.; Burd, S. D.; Cairns, A. J.; Luebke, R.; Forrest, K.; Pham, T.; Ma, S.; Space, B.; Wojtas, L.; Eddaoudi, M.; Zaworotko, M. J. Porous materials with optimal adsorption thermodynamics and kinetics for CO2 separation. *Nature* **2013**, *495*, 80−84.

(6) Hu, Z.; Deibert, B. J.; Li, J. Luminescent metal-organic frameworks for chemical sensing and explosive detection. *Chem. Soc. Rev.* **2014**, *43*, 5815−5840.

(7) Hu, Z.; Lustig, W. P.; Zhang, J.; Zheng, C.; Wang, H.; Teat, S. J.; Gong, Q.; Rudd, N. D.; Li, J. Effective Detection of Mycotoxins by a Highly Luminescent Metal-Organic Framework. *J. Am. Chem. Soc.* **2015**, *137*, 16209−16215.

(8) An, B.; Li, Z.; Song, Y.; Zhang, J.; Zeng, L.; Wang, C.; Lin, W. Cooperative copper centres in a metal-organic framework for selective conversion of CO2 to ethanol. *Nat. Catal.* **2019**, *2*, 709−717.

(9) Duan, J.; Chen, S.; Zhao, C. Ultrathin metal-organic framework array for efficient electrocatalytic water splitting. *Nat. Commun.* **2017**, *8*, 15341.

(10) Gong, Q.; Hu, Z.; Deibert, B. J.; Emge, T. J.; Teat, S. J.; Banerjee, D.; Mussman, B.; Rudd, N. D.; Li, J. Solution Processable MOF Yellow Phosphor with Exceptionally High Quantum Efficiency. *J. Am. Chem. Soc.* **2014**, *136*, 16724−16727.

(11) Lustig, W. P.; Mukherjee, S.; Rudd, N. D.; Desai, A. V.; Li, J.; Ghosh, S. K. Metal-organic frameworks: functional luminescent and photonic materials for sensing applications. *Chem. Soc. Rev.* **2017**, *46*, 3242−3285.

(12) Carrington, E. J.; McAnally, C. A.; Fletcher, A. J.; Thompson, S. P.; Warren, M.; Brammer, L. Solvent-switchable continuous-breathing behaviour in a diamondoid metal-organic framework and its influence on CO2 versus CH4 selectivity. *Nat. Chem.* **2017**, *9*, 882−889.

(13) Wannapaiboon, S.; Schneemann, A.; Hante, I.; Tu, M.; Epp, K.; Semrau, A. L.; Sternemann, C.; Paulus, M.; Baxter, S. J.; Kieslich, G.; Fischer, R. A. Control of structural flexibility of layered-pillared metal-organic frameworks anchored at surfaces. *Nat. Commun.* **2019**, *10*, 346.

(14) Zhao, P.; Fang, H.; Mukhopadhyay, S.; Li, A.; Rudić, S.; McPherson, I. J.; Tang, C. C.; Fairen-Jimenez, D.; Tsang, S. C. E.; Redfern, S. A. T. Structural dynamics of a metal-organic framework induced by CO2 migration in its non-uniform porous structure. *Nat. Commun.* **2019**, *10*, 999.

(15) Sarkisov, L.; Martin, R. L.; Haranczyk, M.; Smit, B. On the Flexibility of Metal-Organic Frameworks. *J. Am. Chem. Soc.* **2014**, *136*, 2228−2231.

(16) Schneemann, A.; Bon, V.; Schwedler, I.; Senkovska, I.; Kaskel, S.; Fischer, R. A. Flexible metal-organic frameworks. *Chem. Soc. Rev.* **2014**, *43*, 6062−6096.

(17) Chang, Z.; Yang, D.-H.; Xu, J.; Hu, T.-L.; Bu, X.-H. Flexible Metal-Organic Frameworks: Recent Advances and Potential Applications. *Adv. Mater.* **2015**, *27*, 5432−5441.

(18) Yu, M.-H.; Space, B.; Franz, D.; Zhou, W.; He, C.; Li, L.; Krishna, R.; Chang, Z.; Li, W.; Hu, T.-L.; Bu, X.-H. Enhanced Gas Uptake in a Microporous Metal-Organic Framework via a Sorbate Induced-Fit Mechanism. *J. Am. Chem. Soc.* **2019**, *141*, 17703−17712.

(19) Mason, J. A.; Oktawiec, J.; Taylor, M. K.; Hudson, M. R.; Rodriguez, J.; Bachman, J. E.; Gonzalez, M. I.; Cervellino, A.; Guagliardi, A.; Brown, C. M.; Llewellyn, P. L.; Masciocchi, N.; Long, J. R. Methane storage in flexible metal-organic frameworks with intrinsic thermal management. *Nature* **2015**, *527*, 357−361.

(20) Yue, Y.; Rabone, J. A.; Liu, H.; Mahurin, S. M.; Li, M.-R.; Wang, H.; Lu, Z.; Chen, B.; Wang, J.; Fang, Y.; Dai, S. A Flexible Metal-Organic Framework: Guest Molecules Controlled Dynamic Gas Adsorption. *J. Phys. Chem. C* **2015**, *119*, 9442−9449.

(21) Bourrelly, S.; Llewellyn, P. L.; Serre, C.; Millange, F.; Loiseau, T.; Férey, G. Different Adsorption Behaviors of Methane and Carbon Dioxide in the Isotypic Nanoporous Metal Terephthalates MIL-53 and MIL-47. *J. Am. Chem. Soc.* **2005**, *127*, 13519−13521.

(22) Uemura, K.; Yamasaki, Y.; Komagawa, Y.; Tanaka, K.; Kita, H. Two-Step Adsorption/Desorption on a Jungle-Gym-Type Porous Coordination Polymer. *Angew. Chem., Int. Ed.* **2007**, *46*, 6662−6665.

(23) Cho, H. S.; Yang, J.; Gong, X.; Zhang, Y.-B.; Momma, K.; Weckhuysen, B. M.; Deng, H.; Kang, J. K.; Yaghi, O. M.; Terasaki, O. Isotherms of individual pores by gas adsorption crystallography. *Nat. Chem.* **2019**, *11*, 562−570.

(24) Krause, S.; Bon, V.; Senkovska, I.; Stoeck, U.; Wallacher, D.; Többens, D. M.; Zander, S.; Pillai, R. S.; Maurin, G.; Coudert, F.-X.; Kaskel, S. A pressure-amplifying framework material with negative gas adsorption transitions. *Nature* **2016**, *532*, 348−352.

(25) Sung Cho, H.; Deng, H.; Miyasaka, K.; Dong, Z.; Cho, M.; Neimark, A. V.; Ku Kang, J.; Yaghi, O. M.; Terasaki, O. Extra adsorption and adsorbate superlattice formation in metal-organic frameworks. *Nature* **2015**, *527*, 503−507.

(26) Henke, S.; Schmid, R.; Grunwaldt, J.-D.; Fischer, R. A. Flexibility and Sorption Selectivity in Rigid Metal-Organic Frameworks: The Impact of Ether-Functionalised Linkers. *Chem. - Eur. J.* **2010**, *16*, 14296−14306.

(27) Henke, S.; Schneemann, A.; Wütscher, A.; Fischer, R. A. Directing the Breathing Behavior of Pillared-Layered Metal-Organic Frameworks via a Systematic Library of Functionalized Linkers Bearing Flexible Substituents. *J. Am. Chem. Soc.* **2012**, *134*, 9464−9474.

(28) Nijem, N.; Thissen, P.; Yao, Y.; Longo, R. C.; Roodenko, K.; Wu, H.; Zhao, Y.; Cho, K.; Li, J.; Langreth, D. C.; Chabal, Y. J. Understanding the Preferential Adsorption of CO2 over N2 in a Flexible Metal-Organic Framework. *J. Am. Chem. Soc.* **2011**, *133*, 12849−12857.

(29) Banerjee, D.; Wang, H.; Plonka, A. M.; Emge, T. J.; Parise, J. B.; Li, J. Direct Structural Identification of Gas Induced Gate-Opening Coupled with Commensurate Adsorption in a Microporous Metal-Organic Framework. *Chem. - Eur. J.* **2016**, *22*, 11816−11825.

(30) Huang, R.-W.; Wei, Y.-S.; Dong, X.-Y.; Wu, X.-H.; Du, C.-X.; Zang, S.-Q.; Mak, T. C. W. Hypersensitive dual-function luminescence switching of a silver-chalcogenolate cluster-based metal-organic framework. *Nat. Chem.* **2017**, *9*, 689−697.

(31) Wang, Q.; Ke, T.; Yang, L.; Zhang, Z.; Cui, X.; Bao, Z.; Ren, Q.; Yang, Q.; Xing, H. Separation of Xe from Kr with Record Selectivity and Productivity in Anion-Pillared Ultramicroporous Materials by Inverse Size-Sieving. *Angew. Chem., Int. Ed.* **2020**, *59*, 3423−3428.

(32) Banerjee, D.; Simon, C. M.; Plonka, A. M.; Motkuri, R. K.; Liu, J.; Chen, X.; Smit, B.; Parise, J. B.; Haranczyk, M.; Thallapally, P. K. Metal−organic framework with optimally selective xenon adsorption and separation. *Nat. Commun.* **2016**, *7*, 11831.

https://dx.doi.org/10.1021/jacs.0c09475
J. Am. Chem. Soc. 2020, 142, 20088−20097

(33) Banerjee, D.; Cairns, A. J.; Liu, J.; Motkuri, R. K.; Nune, S. K.; Fernandez, C. A.; Krishna, R.; Strachan, D. M.; Thallapally, P. K. Potential of Metal-Organic Frameworks for Separation of Xenon and Krypton. *Acc. Chem. Res.* **2015**, *48*, 211−219.
(34) Li, L.; Guo, L.; Zhang, Z.; Yang, Q.; Yang, Y.; Bao, Z.; Ren, Q.; Li, J. A Robust Squarate-Based Metal-Organic Framework Demonstrates Record-High Affinity and Selectivity for Xenon over Krypton. *J. Am. Chem. Soc.* **2019**, *141*, 9358−9364.
(35) Wang, H.; Yao, K.; Zhang, Z.; Jagiello, J.; Gong, Q.; Han, Y.; Li, J. The first example of commensurate adsorption of atomic gas in a MOF and effective separation of xenon from other noble gases. *Chem. Sci.* **2014**, *5*, 620−624.
(36) Chen, X.; Plonka, A. M.; Banerjee, D.; Krishna, R.; Schaef, H. T.; Ghose, S.; Thallapally, P. K.; Parise, J. B. Direct Observation of Xe and Kr Adsorption in a Xe-Selective Microporous Metal-Organic Framework. *J. Am. Chem. Soc.* **2015**, *137*, 7007−7010.
(37) Jiang, Z.-Q.; Jiang, G.-Y.; Wang, F.; Zhao, Z.; Zhang, J. Controlling State of Breathing of Two Isoreticular Microporous Metal-Organic Frameworks with Triazole Homologues. *Chem. - Eur. J.* **2012**, *18*, 10525−10529.
(38) Fu, H.-R.; Zhang, J. Structural Transformation and Hysteretic Sorption of Light Hydrocarbons in a Flexible Zn-Pyrazole-Adenine Framework. *Chem. - Eur. J.* **2015**, *21*, 5700−5703.
(39) Krause, S.; Hosono, N.; Kitagawa, S. Chemistry of Soft Porous Crystals: Structural Dynamics and Gas Adsorption Properties. *Angew. Chem., Int. Ed.* **2020**, *59*, 15325−15341.
(40) Nijem, N.; Wu, H.; Canepa, P.; Marti, A.; Balkus, K. J.; Thonhauser, T.; Li, J.; Chabal, Y. J. Tuning the Gate Opening Pressure of Metal-Organic Frameworks (MOFs) for the Selective Separation of Hydrocarbons. *J. Am. Chem. Soc.* **2012**, *134*, 15201−15204.
(41) Xiong, S.; Liu, Q.; Wang, Q.; Li, W.; Tang, Y.; Wang, X.; Hu, S.; Chen, B. A flexible zinc tetrazolate framework exhibiting breathing behaviour on xenon adsorption and selective adsorption of xenon over other noble gases. *J. Mater. Chem. A* **2015**, *3*, 10747−10752.
(42) Fernandez, C. A.; Liu, J.; Thallapally, P. K.; Strachan, D. M. Switching Kr/Xe selectivity with temperature in a metal-organic framework. *J. Am. Chem. Soc.* **2012**, *134*, 9046−9049.
(43) Coudert, F.-X.; Jeffroy, M.; Fuchs, A. H.; Boutin, A.; Mellot-Draznieks, C. Thermodynamics of Guest-Induced Structural Transitions in Hybrid Organic-Inorganic Frameworks. *J. Am. Chem. Soc.* **2008**, *130*, 14294−14302.

https://dx.doi.org/10.1021/jacs.0c09475
J. Am. Chem. Soc. 2020, 142, 20088−20097